Enhancing Security in Near-Field Location Division Multiple Access by Variational Quantum Circuit

(Invited Paper)

Quan Minh Nguyen*, Bhaskara Narottama*, Minh-Hien T. Nguyen†, Vishal Sharma†, Quang Nhat Le*, and Trung Q. Duong*†

*Memorial University, Canada, e-mail: {qmnguyen, bnarottama, qnle, tduong}@mun.ca

†Queen's University Belfast, UK, e-mail: {h.nguyen, v.sharma, trung.q.duong}@qub.ac.uk

***Abstract*—Location division multiple access (LDMA), enabled by extremely large-scale antenna arrays (ELAAs), allows user distinction in near-field communications (NFC) based on their spatial locations. By exploiting signal orthogonality in both the angular and distance domains, LDMA achieves precise signal focusing, with unique beamforming vectors assigned to the corresponding users. Leveraging these spatial degrees of freedom to enhance physical-layer-security, we propose a sequential quantum–classical (SQC) workflow to optimize the hybrid beamforming architecture. This workflow jointly maximizes the sum secrecy rate and enables efficient power allocation under quality-of-service (QoS) constraints. To address the resulting high-dimensional, and non-convex optimization problem, the proposed approach incorporates the metaheuristic differential evolution algorithm upon the existing variational quantum circuits (VQC). This integration alleviates quantum computational resource demands while maintaining effective solution-space exploration. Simulation results demonstrate the robustness of the proposed method against eavesdropping attacks, even in worst-case scenarios where legitimate users and eavesdroppers share identical angles of departure (AoD).**

I. Introduction

Next-generation mobile networks (6G) are expected to deliver unprecedented levels of connectivity, ultra-high data rates, and enhanced security in data transmission. To meet these demands, emerging communication systems aim to leverage high-frequency spectrum resources, including millimeter-wave (mmWave) and terahertz (THz) bands, along with massive multiple-input multiple-output (mMIMO) architectures. These technologies promote substantial improvements in spectral efficiency, capacity, and energy efficiency [1]. However, operating at such high frequencies constrains coverage range and adversely impacts link reliability and overall network performance due to substantial free-space path loss [2]. Extremely large-scale antenna arrays (ELAA) have lately been investigated as a viable means to mitigate these propagation challenges. At mmWave and THz frequencies, the short wavelengths enable high antenna-element densities within a compact physical area [3]. This capability results in an enhanced beamforming gain, which compensates for propagation losses and extends transmission range, facilitating reliable high-frequency wireless connections. Moreover, ELAA significantly enlarges the near-field region, which is anticipated to be a key operating regime in next-generation wireless systems [4].

Conventional far-field communications (FFC) employ spatial division multiple access (SDMA) technique, which relies solely on beamsteering, i.e., using the transmission angle to characterize the channel. This approach overlooks the benefits of exploiting both the distance and angular domains to differentiate users, which enables more precise signal focusing and improved spatial resolution, a key feature known as beamfocusing that distinguishes NFC from FFC [5]. As the number of antennas increases, the spatial resolution of NFC approaches an ideal limit, allowing the base station to accurately focus multiple signals on distinct user locations [6]. Leveraging the addtional degree of freedom in the distance domain, LDMA employs beamfocusing with ELAA to provide user-specific beamforming vectors with enhanced interference suppression [6]. To mitigate the hardware complexity and power consumption associated with fully digital architectures, hybrid beamforming designs are often adopted to improve spectrum efficiency and foster secure data transmission, especially in high-density multi-user scenarios.

While NFC introduces an additional degree of freedom to direct signals toward intended users, the broadcast nature of wireless channels still exposes systems to nearby untrusted users. This vulnerability has fueled interest in physical layer security (PLS), which exploits the unique properties of the wireless medium to mitigate security threats, including eavesdropping, as emphasized in works such as [7] and [8]. Existing NFC-PLS works primarily focus on optimization and multiple-access methods to enhance security, but generally overlook the potential of LDMA [6], [9], [10]. Exploiting LDMA to its full potential necessitates advanced learning approaches capable of optimizing the high-dimensional hybrid beamforming problem inherent in dense NFC architectures. In this context, quantum-based learning has recently emerged as a promising solution due to its broad applicability and potential for exponential speedup [11]. In particular, quantum computing has demonstrated its capability to address optimization problem such as enhancing data transmission security and improving energy efficiency, as shown in [12], [13]. These findings indicate that quantum-enhanced learning frameworks are well suited for tackling the complexity and security challenges of LDMA-enabled NFC systems.

In this paper, we propose a sequential quantum-classical

(SQC) algorithm to optimize the hybrid beamforming architecture, thereby enhancing the secrecy rate in LDMA-NFC systems. The formulated optimization problem is highly challenging, as it involves strongly coupled variables arising from hybrid beamforming, spherical-wave channel characteristics, and non-convex secrecy-rate formulations. To ease the quantum resource requirements associated with the beamforming optimization, we incorporate a classically-computed, heuristic differential evolution alongside a variational quantum circuit.

II. System Model and Problem Formulation

A downlink multiple-input single-output (MISO) near-field system is investigated, in which a base station (BS) is equipped with N_T antennas arranged in a uniform linear array (ULA) layout. The antenna elements are indexed by $n \in \{0, 1, \ldots, N_T\}$ where $N_T = 2N + 1$. The inter-element spacing is set to $d = \frac{\lambda}{2}$, where λ represents the carrier wavelength. The BS simultaneously sends $\mathbf{s} \in \mathbb{C}^{K\times 1}$ data streams to K legitimate users in the near-field region that also includes a potential eavesdropper, where $\mathbb{E}\{\mathbf{s}^H\mathbf{s}\} = \mathbf{I}_K$. The eavesdropper is modeled as an untrusted user without requiring prior identification of the malicious user. This assumption enables the development of secure transmission strategies that are robust to any user attempting to decode confidential information. Fig. 1 illustrates the near-field ULA-ELAA system. The boundary of the near-field region is defined by the Rayleigh distance, given by $d_R = \frac{2D^2}{\lambda}$ where D is the antenna aperture. To ensure independent data streams, it is essential that $K \leq N_{RF}$, where N_{RF} denotes the number of radio frequency (RF) chains. For the sake of simplicity, $K = N_{RF}$ is used throughout this paper, following studies such as [6] and [14].

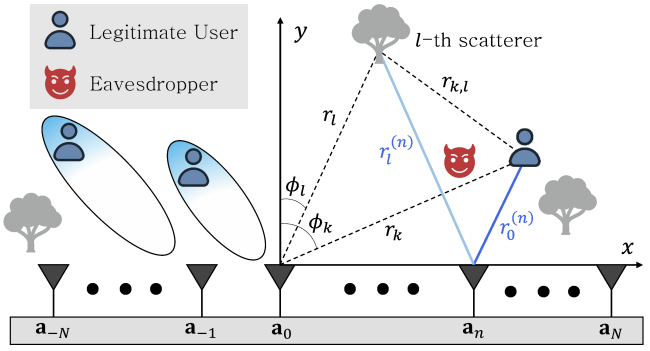

Fig. 1. The assumed system model, equipped with a near-field ULA-ELAA configuration, under potential eavesdropping.

A. Near-field Channel Model

In practical wireless propagation environments, L scatterers are typically present, introducing non-line-of-sight (NLoS) paths in addition to direct line-of-sight (LoS) transmission. Let $\mathbf{a}_{\delta_n} = [\delta_n d, 0]^T$ be the Cartesian coordinate of the n-th antenna, where $\delta_n = n - N$ denotes the index offset from the central array element. The positions of the k-th user and the l-th scatterer are, respectively, denoted by $\mathbf{u}_k = [r_k \sin\phi_k, r_k \cos\phi_k]^T$ and $\mathbf{z}_l = [r_l \sin\phi_l, r_l \cos\phi_l]^T$, with ϕ_k and ϕ_l representing the AoD from the BS to the k-th user and l-th scatterer, respectively. Here, r demonstrates the distance between the center of the transmitting array and the user (or scatterer). Accordingly, the propagation distance between the n-th antenna and the k-th user (or l-th scatterer) can be given by

$$\begin{aligned} r_l^{(n)} &= \sqrt{r^2 + \delta_n^2 d^2 - 2r\delta_n d \sin\phi} \\ &\approx r - \delta_n d \sin\phi + \frac{\delta_n^2 d^2 \cos^2\phi}{2r}, \end{aligned} \tag{1}$$

where the approximation is obtained by taking the first three terms from the Fresnel approximation [15], with $\sqrt{1+x} \approx 1 + \frac{x}{2} - \frac{x^2}{8}$ for $x = \frac{\delta_n^2 d^2 - 2r\delta_n d \sin\phi}{r^2}$. According to superposition principle [16], the channel between the transmitter and the k-th user can be described as

$$\mathbf{h}_k = \alpha_0 g_0 \mathbf{b}(r_0^{(n)}, \phi_0) + \frac{1}{\sqrt{L}} \sum_{l=1}^{L} \alpha_l g_l \mathbf{b}(r_l^{(n)}, \phi_l) e^{j\theta_{k,l}}, \tag{2}$$

where $g_0 = \sqrt{\frac{K_{Ri}}{K_{Ri}+1}}$ represents the complex channel gain for the LoS path and K_{Ri} is the Rician fading factor. The NLoS path gains $g_l \sim \mathcal{CN}(0, \sigma_{\alpha_l}^2)$ are assumed to be independent and identically distributed (i.i.d), with variance $\sigma_{\alpha_l}^2 = \frac{1}{K_{Ri}+1}$. The random phase of the l-th scatterer path to the k-th user follows a uniform distribution, $\theta_{k,l} \sim \mathcal{U}(0, 2\pi)$ [17]. The signal experiences free-space path loss α_l over the two-hop transmission distance $r_l^{(n)}$ and $r_{k,l}$, where $r_{k,l}$ is the distance between the k-th user and l-th scatterer. In NFC, the spherical wavefront characteristics enable enhanced spatial resolution at a specific location (r, ϕ). Exploiting this property, ELAA focuses signals on k-th user by employing beamfocusing vectors $\mathbf{b}(r_l^{(n)}, \phi_l)$ from every antenna, which can be expressed as $[\mathbf{b}(r_l^{(n)}, \phi_l)]_n = e^{-j\frac{2\pi}{\lambda}\left(-\delta_n d \sin\phi + \frac{\delta_n^2 d^2 \cos^2\phi}{2r}\right)}$. As the number of antennas increases, the unit-norm beamfocusing vectors to two different locations (r_a, ϕ_a) and (r_b, ϕ_b) become asymptotically orthogonal under the increasing limit of aperture, i.e., $N_T \to +\infty$, as follows [6]:

$$\lim_{N_T\to+\infty} |\mathbf{b}^H(r_a, \phi_a)\mathbf{b}(r_b, \phi_b)| = 0, \quad \text{for } r_a \neq r_b \text{ and } \phi_a \neq \phi_b. \tag{3}$$

This lays the ground for LDMA which distinguishes the users through both spatial and angular domains, reducing inter-user interference.

B. Hybrid Beamforming Architecture

This paper considers a fully connected discrete phase-shifter-based hybrid beamforming architecture, where N_{RF} RF chains serving K users, subject to the practical hardware constraint $N_{RF} \leq N_T$ [6], [16]. Initially, a digital beamformer $\mathbf{W}_D \in \mathbb{C}^{N_{RF}\times K}$ processes the original signal in the baseband to direct it towards the intended users while mitigating inter-user interference. Then, each signal s_k is converted to the RF domain via its corresponding RF chain before being processed

by the analog beamformer $\mathbf{W}_A \in \mathbb{C}^{N_T \times N_{RF}}$. Phase shifters in the analog beamformer subsequently adjust the phase of each antenna element, precisely directing the signal to the intended users. This mechanism allows independent optimization for the digital and analog beamformers to enhance overall system performance.

Considering the additive white Gaussian noise (AWGN) $\mathbf{n} \sim \mathcal{CN}(0, \sigma^2 \mathbf{I}_K) \in \mathbb{C}^{K \times 1}$, the observed signals at the k-th legitimate user can be given by $y_k = \mathbf{h}_k^H \mathbf{W}_A \mathbf{W}_D \mathbf{s} + n_k$, where $\mathbf{y} = [y_1, y_2, \ldots, y_K]$. $\mathbf{H}_K = [h_1, h_2, \ldots, h_K]^H \in \mathbb{C}^{K \times N_T}$ describes the channel matrix whose element follows (2). The achievable data rate at k-th user can be written as

$$R_k = \log_2\Big(1 + \frac{|\mathbf{h}_k^H \mathbf{W}_A \mathbf{w}_{D,k}|^2}{\sigma_k^2 + \sum_{m \neq k}^{K} |\mathbf{h}_k^H \mathbf{W}_A \mathbf{w}_{D,m}|^2}\Big), \quad (4)$$

where $\mathbf{w}_{D,k} \in \mathbb{C}^{N_{RF} \times 1}$ denotes the digital beamforming vector corresponding to the user k. Meanwhile, the eavesdropper intercepts signals from the k-th user at a data rate $R_{e,k}$, determined by

$$R_{e,k} = \log_2\Big(1 + \frac{|\mathbf{h}_e^H \mathbf{W}_A \mathbf{w}_{D,k}|^2}{\sigma_e^2 + \sum_{m \neq k}^{K} |\mathbf{h}_e^H \mathbf{W}_A \mathbf{w}_{D,m}|^2}\Big), \quad (5)$$

where $\mathbf{h}_e \in \mathbb{C}^{N_T \times 1}$ follows (2) considering the location of the e-th eavesdropper, given by $\mathbf{v}_e = [r_e \cos\phi_e, r_e \sin\phi_e]^T$. The secrecy rate quantifies downlink security by measuring the difference between the achievable data rate of a legitimate user, R_k, and that of a potential eavesdropper, $R_{e,k}$. For the k-th legitimate user in the presence of the e-th eavesdropper, it is expressed as $\chi_k = [R_k - R_{e,k}]^+$, where the term $[\alpha]^+ = \max\{0, \alpha\}$ is used as secrecy rate which cannot be negative [18]. If χ_k becomes zero, the system fails to prevent the e-th eavesdropper from decoding the signal s_k intended for the k-th legitimate user, at a rate equal to or exceeding that of the k-th user.

C. Secrecy Problem Formulation

This paper addresses the joint optimization of the sum secrecy rate across all K legitimate users and power allocation by finetuning the hybrid beamforming architecture, while satisfying the QoS constraint. The optimization problem is formulated as follows:

$$\max_{\mathbf{w}_{D,k}, \mathbf{w}_{RF,j}} \sum_{k=1}^{K} \chi_k \quad (6a)$$

$$\text{s.t. } \chi_k \geq \chi_{min}, \forall k, \quad (6b)$$

$$0 < P \leq P_{max}, \quad (6c)$$

$$|[\mathbf{W}_A]_{j,n}| = 1, \forall j, n, \quad (6d)$$

where $P = \|\mathbf{W}_A \mathbf{W}_D\|_F$ is the total power allocation and the entry $[\mathbf{W}_A]_{j,n}$ corresponds to the j-th RF chain and the n-th antenna element. Constraint (6b) ensures each user's QoS requirement. Constraint (6c) limits the maximum transmitted power of the BS. Since phase shifters only adjust the phase of the signal without affecting its magnitude, constraint (6d) ensures that each analog beamforming vector $[\mathbf{W}_A]_{j,n}$ is unit-modulus entry with normalized power.

III. Sequential Quantum-Classical Solution

In this section, we propose a sequential quantum-classical (SQC) algorithm to optimize the hybrid beamforming architecture. First, the analog beamformer $\mathbf{W}_A$ is enhanced using differential evolution (DE), a population-based stochastic method that balances exploration and exploitation to approach the global optimum. The optimal $\mathbf{W}_A$, along with the channel state information $\mathbf{H}_K$, is then used to initialize a variational quantum optimizer (VQO), enabling faster convergence and a high-performance design of the digital beamformer $\mathbf{W}_D$. The channel state information is obtained via pilot-based channel probing and stored as classical data for input to the proposed algorithm, whose steps are summarized in Fig. 2.

A. DE-based Analog Beamformer Design

To address the high-dimensional analog beamforming design problem incurred by ELAA, DE is utilized to jointly optimize the design of the analog beamformer and power allocation, while keeping the digital beamformer $\mathbf{W}_D$ fixed.

Initialization: The DE algorithm initializes a population of M feasible analog beamforming matrices $\mathbf{W}_{A,id}$, denoted by $\mathcal{P}^{[0]} = \{\mathbf{W}_{A,1}, \ldots, \mathbf{W}_{A,M}\}$. Each individual $\mathbf{W}_{A,id}$ is generated by setting $[\mathbf{W}_{A,id}]_{n,j}^{[0]} = \exp(i2\pi\tilde{x}_{n,j}^{[0]})$.

Mutation: At generation τ, mutant analog beamforming matrices are generated upon the current population as $\mathbf{V}_{A,id}^{[\tau]} = \angle\{\mathbf{W}_{A,best}^{[\tau]} + \zeta \times (\mathbf{W}_{A,r1}^{[\tau]} - \mathbf{W}_{A,r2}^{[\tau]})\}$, where ζ is the differential weight factor. $\mathbf{W}_{A,r1}^{[\tau]}$ and $\mathbf{W}_{A,r2}^{[\tau]}$ are randomly chosen from the population $\mathcal{P}^{[\tau]}$, and $\mathbf{W}_{A,best}^{[\tau]}$ is the optimal solution in terms of the fitness function $\mathcal{F}$, described as

$$\begin{aligned}&\mathcal{F}(\mathbf{W}_{A,id}) \\ &= \underbrace{\underbrace{-\sum_{k=1}^{K} \chi_k}_{f(\mathbf{W}_{A,id})} + \Big(\epsilon_{DE,1} \sum_{k=1}^{K} \omega(\chi_k) + \epsilon_{DE,2} \rho(P_{id})\Big)}_{F(\mathbf{W}_{A,id})} \\ &+ \eta(\mathbf{W}_{A,id}), \end{aligned} \quad (7)$$

where the first term motivates the improvements of the secrecy rate defined in (6a). The second term imposes the penalty when the constraints of (6b) and (6c) are not satisfied, with weights $\epsilon_{DE,1}$ and $\epsilon_{DE,2}$. The corresponding penalty functions can be defined as

$$\omega(\chi_k) = \begin{cases} \chi_{min} - \chi_k, & \text{for } \chi_k < \chi_{min}, \\ 0, & \text{for } \chi_k \geq \chi_{min}, \end{cases} \quad (8a)$$

$$\rho(P_{id}) = \begin{cases} 0, & \text{for } P \leq P_{max}, \\ P - P_{max}, & \text{for } P > P_{max}, \end{cases} \quad (8b)$$

where P_{id} denotes the total transmit power associated with the analog beamformer $\mathbf{W}_{A,id}$. We adopt the superiority feasible points (SFP) scheme [19] to ensure that infeasible individuals $\mathbf{W}_{A,x} \in P_{infs}$ in a population $P^{[\tau]}$ always have worse

fitness values than feasible ones $\mathbf{W}_{A,y} \in P_{fs}$, with additional punishment $\eta(W_{A,id})$ given in (9), where $\mathcal{P}^{[\tau]} = \mathcal{P}^{[\tau]}_{fs} \cup \mathcal{P}^{[\tau]}_{infs}$.

Crossover: To enhance population diversity, we merge the entries of each individual with those of its corresponding mutant matrix, to produce potential offspring. Specifically, a trial matrix $\mathbf{U}^{[\tau]}_{A,ind} \in \mathbb{C}^{N_T \times N_{RF}}$ is constructed for each individual under the control of a crossover rate C_r, defined as

$$[\mathbf{U}_{A,id}]^{[\tau]}_{n,j} = \begin{cases} [\mathbf{V}^{[\tau]}_{A,id}]_{n,j} & \text{if } rand \leq C_r \text{ or } (n,j) = (n^*, j^*), \\ [\mathbf{W}^{[\tau]}_{A,id}]_{n,j} & \text{otherwise,} \end{cases} \tag{10}$$

where (n^*, j^*) is a randomly selected entry to ensure at least one component originates from $\mathbf{V}_{A,ind}$, and "$rand \in [0,1]$" denotes an independent uniform random number.

Selection: During the selection phase, a new analog beamforming individual $\mathbf{W}^{[\tau+1]}_{A,ind}$ is formulated by comparing the fitness value of the corresponding trial matrix $\mathbf{U}^{[\tau]}_{A,id}$ against that of the target matrix $\mathbf{W}^{[\tau]}_{A,ind}$, as follows:

$$\mathbf{W}^{[\tau+1]}_{A,id} = \begin{cases} \mathbf{U}^{[\tau]}_{A,id} & \text{if } \mathcal{F}(\mathbf{U}^{[\tau]}_{A,id}) < \mathcal{F}(\mathbf{W}^{[\tau]}_{A,id}), \\ \mathbf{W}^{[\tau]}_{A,id} & \text{otherwise.} \end{cases} \tag{11}$$

After evolving the candidate population through τ_{max} iterations of mutation, crossover, and selection, the DE algorithm yields an optimal analog beamformer $\mathbf{W}^{[t]}_A = \text{argmin}_{\mathbf{W}_{A,id}} \mathcal{F}$, for $\mathbf{W}_{A,id} \in \mathcal{P}^{[\tau_{max}]}$.

B. VQO-Based Digital Beamformer Design.

A VQC comprises three layers: a data encoding layer that maps classical inputs into quantum states, a parameterized layer with tunable rotation and entangling gates to flexibly manipulate the quantum states, a measurement layer that collapses quantum states into classical outputs. The integration of a classical optimizer, typically a gradient-based method, with a VQC formulates a variational quantum optimizer (VQO). This framework is capable of fine-tuning the circuit parameters through iterative optimization, which enables the system to learn optimal solutions to complex problems.

Initialization: The encoding layer maps the classical channel information $\mathbf{H}_K$ and the analog precoder $\mathbf{W}_A$ from III-A into a quantum reference state. Specifically, we compute $\mathbf{G}^{[t]}_{KN_{RF}} = \mathbf{H}^H_K \mathbf{W}^{[t]}_A$ and then flatten the matrix into $\mathbf{G}^{[t]}_f = \{\mathbf{x}_1, \ldots, \mathbf{x}_{KN_{RF}}\}$. The reference state is obtained by encoding the classical information $\mathbf{x}_q \in \mathbf{G}^{[t]}_f$ into the computational basis state $|0\rangle^{\otimes Q}$ as $|\psi_r\rangle = U_E |0\rangle^{\otimes Q}$, where U_E is the encoding operator, defined as

$$U_E = \bigotimes_q^{Q/2} R_Y^{(2q-1)}(\mathcal{R}(\mathbf{x}_q)) R_Z^{(2q)}(\mathcal{I}(\mathbf{x}_q)) H^{\otimes Q}, \tag{12}$$

where $Q = 2N_{RF}K$ denotes the number of qubits. First, Hadamard gates map the ground state $|0\rangle^{\otimes Q}$ into a uniform superposition state, as follows $|\psi_1\rangle = H^{\otimes Q} |0\rangle^{\otimes Q} = \frac{1}{\sqrt{2^Q}} \sum_{x=0}^{2^Q-1} |x\rangle$, where all the computational basis states have the same probability of $\frac{1}{2^Q}$. Then, the classical information are encoded as rotation angles in R_Y and R_Z gates. The resulted reference state provides initial guidance for the VQC, thereby significantly accelerating the quantum learning process.

Training: In the parameterized layer, the initial reference state is transformed through a trainable, parameterized unitary operator U_P with multiple parameterized layer, $U^{(\ell)}$, producing the parameterized state $|\psi_p\rangle = U_P(\boldsymbol{\theta}) |\psi_r\rangle = \prod_{\ell=1}^{\mathcal{L}} U_P^{(\ell)}(\boldsymbol{\theta}_\ell) |\psi_r\rangle$, where each layer operation is formulated by the rotation gate R_Y, and the controlled-NOT (CNOT) gate as

$$U_P^{(\ell)} = U_{ent}^{(\ell)} \cdot U_{rot}^{(\ell)}, \tag{13}$$

where

$$U_{ent}^{(\ell)} = \prod_{q=1}^{Q} \text{CNOT}_{(q,\,(q+1) \bmod Q)}, \tag{14a}$$

$$U_{rot}^{(\ell)} = \bigotimes_{q=1}^{Q} R_Y^{(q)}(\theta_{\ell,q}), \tag{14b}$$

$U_{ent}^{(\ell)}$ and $U_{rot}^{(\ell)}$ represent the entangling and learnable rotational operations, respectively, within each layer ℓ. In each iteration r, the parameterized state $|\psi_P\rangle$ is measured by the Pauli-Z operator which collapses the qubit pairs $(2q-1, 2q)$ into classical information $\mathcal{R}(\mathbf{z}_{j,k})$ and $\mathcal{I}(\mathbf{z}_{j,k})$, respectively, where $\mathbf{z}_{j,k}$ is a matrix entry of the digital beamformer $\mathbf{W}^{[r]}_D$, for $j \in \{1, \ldots, N_{RF}\}$ and $k \in \{1, \ldots, K\}$. The circuit's measurement output is utilized to minimize the loss function, defined as $\mathsf{L}^{(r)} = -\sum_{k=1}^{K} \chi_k - \sum_{k=1}^{K} \vartheta_{\text{rate}}(\chi_k) - \frac{\chi_M}{\chi_{min}} \chi_m$, where the second term imposes a log-barrier penalty to enforce compliance with the constraint defined in (6b). This penalty function can be described as $\vartheta_{\text{rate}}(\chi_k) = \epsilon_{VQO} \log(\max(\chi_k, \beta))$. where β denotes the punishment factor (i.e., $\beta = 10^{-8}$). The third term maintains the fairness between the highest and lowest user rates, denoted by χ_M and χ_m, respectively, once (6b) is not satisfied. Whenever an undesired early termination $\sum_i \chi_i = 0$ occurs, we reinitialize the training process with different starting point. At the end of each iteration, a gradient-based optimizer employs parameter-shift rule to optimize the learnable parameter $\boldsymbol{\theta}$ [20]. This iterative procedure proceeds for r_{max} iterations, enhancing the quantum state $|\psi_P\rangle$ to produce an optimal digital beamformer while respecting the fairness and constraint conditions.

Obtaining the digital beamforming matrix: Given the output vector of the quantum learning model at iteration r as $\mathbf{z}^{[r]} = [z^{[r]}_q]^Q_{q=1}$, where $z^{[r]}_q \in [-1, 1]$, each (j,k)-th element of the digital beamforming matrix $\mathbf{W}^{[r]}_D$ can be obtained as: $\mathbf{w}^{[r]}_{j,k} = z_{2q-1} + i z_{2q}$ for $q \in \{1, \ldots, Q/2\}$, $\mathbf{w}^{[r]}_{j,k} \in \mathbf{W}^{[r]}_D$, $\forall j, k$. Ensuring (6b) is satisfied, $\mathbf{W}^{[r]}_D \leftarrow \frac{P_{max} \mathbf{W}^{[r]}_D}{\|\mathbf{W}^{[t]}_A \mathbf{W}^{[r]}_D\|_F}$ [21]. The resulting digital beamformer $\mathbf{W}^{[r]}_D$ can be directly used for the objective in (6a).

$$\eta(W_{A,id}) = \begin{cases} \max\{0, \max_{\mathbf{W}_{A,y} \in \mathcal{P}_{fs}} f(\mathbf{W}_{A,y}) - \min_{\mathbf{W}_{A,x} \in \mathcal{P}_{infs}} F(\mathbf{W}_{A,x})\} & \text{if } \mathcal{P}_{fs} \neq \varnothing \text{ and } W_{A,id} \in \mathcal{P}_{infs}, \\ 0 & \text{otherwise.} \end{cases} \tag{9}$$

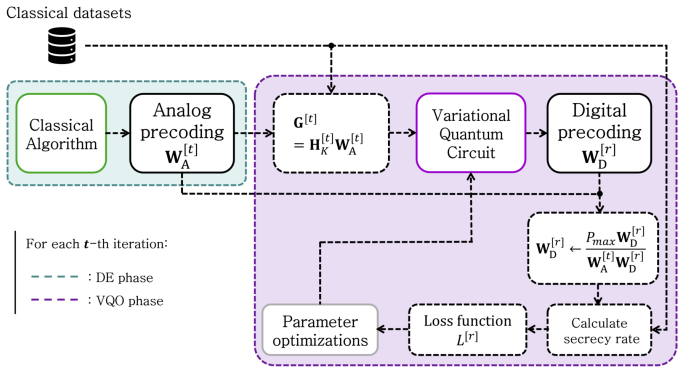

Fig. 2. The process of the proposed SQC workflow.

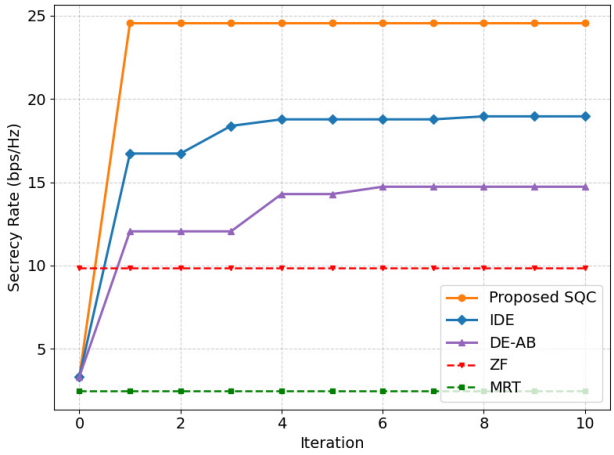

Fig. 3. Secrecy rate performance of the proposed schemes against eavesdropping threat.

IV. Simulation Results and Discussions

In this section, we provide the simulation results for the proposed hybrid quantum-classical workflow. The BS uses an ELAA of $N_T = 257$ elements along the x-axis at 30 GHz. We set the noise power and the maximum power allocation to $\sigma^2 = -105$ dBm and $P_{max} = 30$ dBm, respectively. All the legitimate users are required to achieve the QoS requirement of $\chi_{min} = 1.0$ bps/Hz. The transmitter simultaneously serves two legitimate users at $(20\text{m}, 30°)$ and $(20\text{m}, 60°)$ while avoiding the interception from an eavesdropper at $(10\text{m}, 30°)$, under a realistic multi-path channel model with $L = 3$ NLoS paths. DE phase employs a population of $M = 20$ individuals to ensure sufficient diversity within the search space for analog beamformer and to accelerate the convergence process. Penalty regulators, i.e., $\epsilon_{DE,1} = 200$, $\epsilon_{DE,2} = 2 \times 10^4$, and $\epsilon_{VQO} = 0.5$ guarantee QoS and power allocation requirements. VQO employs Adam optimizer to optimize $\boldsymbol{\theta}$ with a learning rate of $\alpha = 0.05$. We compare the secrecy rate performance of the proposed SQC algorithm over $t = 10$ iterations, each contains $\tau_{max} = 20$ DE generations and $r_{max} = 100$ VQO iterations.

Besides our proposed approach, we analyze the performance of other models, as described in the following. i) Iterative differential evolution (IDE) algorithm. It utilizes the nature-inspired operators of the DE technique to iteratively optimize the analog and digital beamformers, enabling efficient hybrid beamforming. ii) Differential evolution-based analog beamformer (DE-AB). It employs the DE algorithm to adjust the phase shifters of the analog beamformer, while the digital beamformer is initialized randomly. iii) Maximum ratio transmission (MRT). It maximizes the received signal power at each intended user, with beamforming vectors defined as $\mathbf{w}_k = \frac{\mathbf{h}_k}{\|\mathbf{h}_k\|}$. iv) Fully-digital zero-forcing (ZF). It is aimed to eliminate inter-user interference through fully-digital precoding, expressed as $\mathbf{W} = \mathbf{H}_K^H(\mathbf{H}_K\mathbf{H}_K^H)^{-1}$.

Fig. 3 illustrates the convergence performance of the proposed and baseline schemes. The proposed SQC algorithm achieves an early convergence with the highest secrecy performance. For instance, it attains the secrecy rates of approximately 24.5 bps/Hz as early as the first and second iterations. In comparison, DE-AB only achieves the secrecy rates of about 12 bps/Hz at the same iterations. Although the IDE and DE-AB schemes outperform conventional benchmarks (MRT and ZF), their convergence is slower, yielding a secrecy rate approximately 20% to 30% lower than that of the proposed SQC solution. This demonstrates that the proposed SQC algorithm can efficiently solve the joint optimization problem of system performance and power allocation, emphasizing the computational advantages and convergence speedup provided by quantum computing. This is especially helpful for scenarios demanding quick optimization with limited numbers of iterations, such as in low latency communications and/or real-time environments.

Fig. 4 compares the secrecy rates of the five approaches with respect to the total transmit power of the BS. At low transmit power, i.e., $P_{max} \leq 20$ dBm, the proposed SQC achieves approximately the same secrecy rate as IDE and DE-AB. However, as the transmit power increases, SQC outperforms these two schemes by effectively leveraging power allocation and LDMA to mitigate inter-user interference and direct the signals toward the intended users. At high transmit power, IDE underperforms due to its slower convergence in refining the hybrid beamforming architecture with a fixed number of individuals in the population. This limitation prevents IDE from fully exploiting the available power for optimal performance, resulting in reduced secrecy rates compared to SQC.

V. Conclusion

This paper presents a sequential quantum-classical workflow to facilitate secure data transmission, by maximizing secrecy

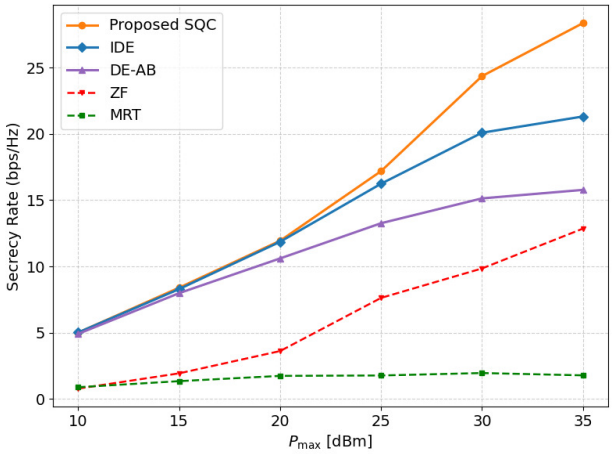

Fig. 4. Secrecy rates versus the maximum power allocation values.

rate, in near-field location division multiple access. The workflow optimizes both the analog and digital beamformers, to maximize the total secrecy rate, while satisfying the QoS constraint and the transmit power budget. Furthermore, to tackle the resulting high-dimensional beamforming posed by ELAA, we employ a hybrid quantum-classical approach, in which the classical, nature-inspired DE algorithm manages the analog beamformer optimization, whereas VQC handles the digital beamformer. This incorporation promotes the exploration of feasible solutions while leveraging quantum advantages and efficiently utilizing computational resources to solve the non-convex optimization problem. Simulation results demonstrate that the proposed SQC algorithm outperforms conventional benchmarks in terms of secrecy rate and convergence speed. These findings highlight the potential of the proposed SQC workflow in enhancing secure and low-latency applications of future communication networks.

REFERENCES

[1] C.-X. Wang, X. You, X. Gao, X. Zhu, Z. Li, C. Zhang *et al.*, "On the road to 6G: Visions, requirements, key technologies, and testbeds," *IEEE Commun. Surv. Tutor.*, vol. 25, no. 2, pp. 905–974, Apr. 2023.

[2] S. Sharma, P. K. Singya, K. Deka, C. Adjih, and M. Sharma, "Terahertz communication: State-of-the-art and future directions," *IEEE Open J. Commun. Soc.*, vol. 6, pp. 6281–6322, Jan. 2025.

[3] S. Ye, M. Xiao, M.-W. Kwan, Z. Ma, Y. H. G. Karagiannidis *et al.*, "Extremely large aperture array (ELAA) communications: Foundations, research advances and challenges," *IEEE Open J. Commun. Soc.*, vol. 5, pp. 7075–7120, Oct. 2024.

[4] W. Saad, M. Bennis, and M. Chen, "A vision of 6G wireless systems: Applications, trends, technologies, and open research problems," *IEEE Netw.*, vol. 34, no. 3, pp. 134–142, May 2020.

[5] H. Zhang, N. Shlezinger, F. Guidi, D. Dardari, M. F. Imani, and Y. C. Eldar, "Beam focusing for near-field multiuser MIMO communications," *IEEE Trans. Wireless Commun.*, vol. 21, no. 9, pp. 7476–7490, Sep. 2022.

[6] Z. Wu and L. Dai, "Multiple access for near-field communications: SDMA or LDMA?" *IEEE J. Sel. Areas Commun.*, vol. 41, no. 6, pp. 1918–1935, Jun. 2023.

[7] ITU-R, *Framework and overall objectives of the future development of IMT for 2030 and beyond*, International Telecommunication Union, Radiocommunication Sector (ITU-R) Recommendation M.2160-0, Nov. 2023.

[8] 3GPP, *Security architecture and procedures for 5G System*, 3rd Generation Partnership Project (3GPP) Technical Specification (TS) TS 33.501, Nov. 2025.

[9] L. Zhang, Y. Wang, H. Chen, and Y. Cao, "Physical-layer security of the NOMA-assisted ISAC systems under near-field scenario," *IEEE Internet Things J.*, vol. 12, no. 12, pp. 18 546–18 553, Jun. 2025.

[10] B. Zhuo, J. Gu, G. Zhang, and H. Yang, "Imperfect resolution of near-field beamfocusing for NOMA-aided physical-layer security," *IEEE Internet Things J.*, vol. 12, no. 12, pp. 18 471–18 483, Jun. 2025.

[11] S. M, "Machine learning and quantum computing for 5G/6G communication networks - a survey," *Int. J. Intell. Netw.*, vol. 3, pp. 197–203, 2022.

[12] S. Park, S. B. Son, S. Jung, and J. Kim, "Dynamic quantum federated learning for UAV-based autonomous surveillance," *IEEE Trans. Vehi. Technol.*, vol. 74, no. 5, pp. 8158–8170, May 2025.

[13] K. Yu, C. Chakraborty, D. Xu, T. Zhang, H. Zhu, O. Alfarraj, and A. Tolba, "Hybrid quantum classical optimization for low-carbon sustainable edge architecture in RIS-assisted AIoT healthcare systems," *IEEE Internet Things J.*, vol. 11, no. 24, pp. 38 987–38 998, Dec. 2024.

[14] M. Liu, C. Pan, K. Zhi, H. Ren, and J. Wang, "Hybrid precoding design for near-field wideband thz systems with spatial non-stationarity," *IEEE Commun. Lett.*, vol. 28, no. 10, pp. 2372–2376, Oct. 2024.

[15] K. T. Selvan and R. Janaswamy, "Fraunhofer and fresnel distances: Unified derivation for aperture antennas," *IEEE Antennas Propag. Mag.*, vol. 59, no. 4, pp. 12–15, Aug. 2017.

[16] Y. Liu, Z. Wang, J. Xu, C. Ouyang, X. Mu, and R. Schober, "Near-field communications: A tutorial review," *IEEE Open J. Commun. Soc.*, vol. 4, pp. 1999–2049, Aug. 2023.

[17] J. Xiao, J. Wang, and Y. Liu, "Channel estimation for pinching-antenna systems (PASS)," *IEEE Commun. Lett.*, vol. 29, no. 8, pp. 1789–1793, Aug. 2025.

[18] M. M. R. andand Limei Peng, "DRL-based physical layer security optimization in near-field MIMO systems," *IEEE Internet Things J.*, vol. 12, no. 12, pp. 18 606–18 615, Jun. 2025.

[19] D. J. Powell and M. M. Skolnick, "Using genetic algorithms in engineering design optimization with non-linear constraints," in *Proc. 5th Int. Conf. Genetic Algorithms*, San Francisco, CA, USA, 1993, p. 424–431.

[20] D. Wierichs, J. Izaac, C. Wang, and C. Y.-Y. Lin, "General parameter-shift rules for quantum gradients," *Quantum*, vol. 6, p. 677, Mar. 2022.

[21] N. T. Nguyen, L. V. Nguyen, N. Shlezinger, A. L. Swindlehurst, and M. Juntti, "Fast deep unfolded hybrid beamforming in multiuser large MIMO systems," in *Proc. Asilomar Conf. Sig., Sys., Comput.*, Pacific Grove, CA, USA, Oct. 2023, pp. 486–490.